analytical chemistry

Article

Cite This: Anal. Chem. XXXX, XXX, XXX−XXX

pubs.acs.org/ac

Versatile Electrochemiluminescence Assays for PEDV Antibody Based on Rolling Circle Amplification and Ru-DNA Nanotags

Jing Ma,[†,‡] Long Wu,[†] Zhonghua Li,[†] Zhicheng Lu,[†] Wenmin Yin,[†] Axiu Nie,[†] Fan Ding,[†] Biru Wang,[†] and Heyou Han*[,†]

[†]State Key Laboratory of Agricultural Microbiology, College of Food Science and Technology, College of Science, Huazhong Agricultural University, Wuhan 430070, People's Republic of China

[‡]College of Life Science, Yangtze University, Jingzhou, Hubei 434023, People's Republic of China

Supporting Information

ABSTRACT: The sensitive and accurate detection methods for PEDV antibody have practical significance for the prevention and treatment of PEDV. In this work, a new multiple pathways signal amplification method was proposed to construct a sensitive electrochemiluminescence (ECL) platform for the detection of PEDV antibody. Using Au NP-modified graphene nanosheet (Au-GN) as the substrate, antibody−antigen reaction as the recognition unit, rolling circle amplification (RCA) for signal enhancement, and assembled cascade Ru-DNA nanotags as signal label, the proposed platform behaved with good specificity and sensitivity. The binding system of biotin−streptavidin, RCA, and $Ru(bpy)_3^{2+}$-doped silica nanoparticles (Ru SNPs) showed remarkable amplification efficiency, low background signal, and little nonspecific adsorption. Moreover, the proposed ECL sensor exhibited good analytical performance for PEDV antibody with a wide linear range from 0.1 pg mL^{-1} to 5000 pg mL^{-1} with a detection limit of 0.05 pg mL^{-1} (S/N = 3). The proposed strategy exhibited the advantages of excellent stability and sensitivity for determination of the PEDV antibody, which was easy to prepare and had a good application prospect.

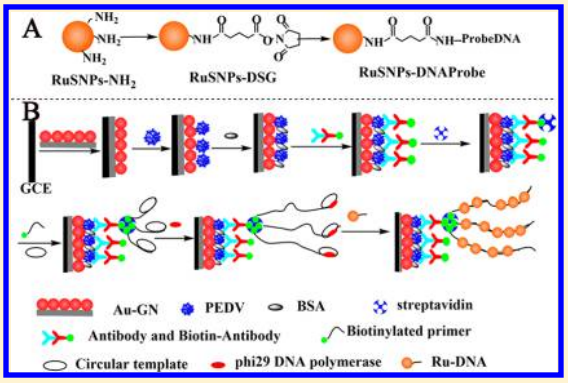

Porcine epidemic diarrhea (PED) was first documented in Europe in 1971, and outbreaks occurred across Europe and expanded into Asia as the disease quickly spread.[1] PED is a highly contagious intestinal infection caused by porcine epidemic diarrhea virus (PEDV) in pigs.[2] This kind of disease has the characteristics of vomiting, acute diarrhea, dehydration, and anorexia in pigs and all ages of neonatal piglets, which resulted in up to 90−95% mortality in suckling pigs.[3,4] Moreover, PEDV could cause enteric disease with a devastating impact on the swine industry. Therefore, it is extremely important and necessary to establish a simple, fast, and accurate method for detecting PEDV antibody because antibody has a practical significance for PEDV diagnosis, wherein traditional methods, including ELISA[5] and (immunofluorescence assay) IFA,[6] are commonly used for PEDV detection. However, these methods possess the limitations of utilizing complex instruments, having tedious operations, and being time consuming. Thus, it is indispensable to develop new methods to make up for those shortcomings.

Electrochemiluminescence (ECL), as an emerging analytical method, is a process by which the electrode surface generates species that undergo exergonic electron transfer reaction and then form excited states that emit light.[7−9] Due to the advantages of wide dynamic range, high sensitivity, stability, facility, and simplicity,[10] ECL has been widely used in all kinds of fields such as immunoassay,[11−13] mycotoxins,[14] DNA analysis,[15] cancer cell (aptamer)[16,17] and metal ion detection,[18] and so on. In the construction of ECL sensors, it is important to choose appropriate signal labels to achieve high sensitivity and stability. Meanwhile, recent studies in the signal amplification strategy mainly focused on enzyme-based nanomaterial-enhanced or DNA-hybridized amplification.[19] Among them, $Ru(bpy)_3^{2+}$ has received great interest due to its superior biocompatibility, high ECL efficiency, and chemical stability.[20−22] Besides, silicon nanoparticles are good substrates for the immobilization of $Ru(bpy)_3^{2+}$, and Ru SNPs are widely applied in bioanalysis.[23−27]

Moreover, the functionalization of graphene oxide with Au NPs provided a large specific surface area, which could immobilize high amounts of protein and display great improvement in signal transmission.[19] Rolling-circle amplification (RCA) driven by DNA polymerase can replicate circularized oligonucleotide probes with either linear or geometric kinetics under isothermal conditions.[28] DNA amplification facilitates the development of immunosensors, especially in sensitivity, by introducing current DNA amplified

Received: February 22, 2018
Accepted: May 23, 2018
Published: May 23, 2018

DOI: 10.1021/acs.analchem.8b00853
Anal. Chem. XXXX, XXX, XXX−XXX

strategies such as hybridization chain reaction (HCR), RCA, and nuclease-assisted target recycling.[29,30] Recently, RCA has been reported in various research methods including the ECL-based technique,[31] the fluorescence method,[32] surface enhanced Raman scattering (SERS),[33] the on-chip method,[34] and electrochemical sensors.[35] Therefore, it is interesting to combine the ideas of RCA, Ru SNPs, Au NPs, and graphene nanosheet (GN) to construct ECL biosensors with good selectivity and high sensitivity.

In this work, a new multiple pathways signal amplification strategy was proposed to achieve a simple, sensitive analysis platform for the quantitative analysis of PEDV antibody. As presented in Scheme 1, Au-GN was first deposited onto a glass carbon electrode surface to immobilize PEDV (Ag) through the strong surface adsorption force of Au-GN hybrids. Next, streptavidin was added to connect biotinylated IgG and biotinylated single-strand RCA primers for binding of the circular template. After the addition of phi29 DNA polymerase and nucleotides, RCA began to produce single-strand micrometer-long DNA. The single long DNA contained lots of tandem-repeat sequences, which could be loaded by linear periodic assembly of DNA complementary detection probes. In this way, Ru-DNA probes could bind specifically to the long strand linear DNA and produce strong ECL signal. Finally, the proposed strategy was applied in the dilution detection of PEDV serum samples, which showed a remarkable ECL response in the detection of PEDV antibody.

Scheme 1. Schematic Representation of (A) the Synthesis of Ru SNP-DNA Probe and (B) Working Principle of RCA ECL Sensing Platform

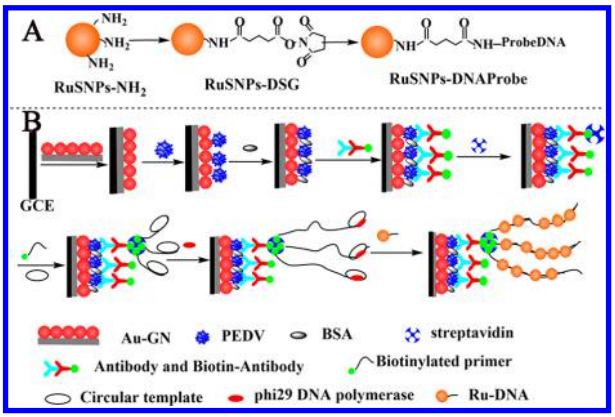

EXPERIMENTAL SECTION

Synthesis of Au-GN Hybrids and Ru SNP-DNA Probe. The synthetic methods of Au-GN hybrids were carried out according to the previous literature.[36−38] Details of the preparation procedures are available in the Supporting Information, SI. Ru SNPs were prepared using a reverse microemulsion method reported by Song's group.[39] In brief, 1-hexanol (1.6 mL), Triton X-100 (1.8 mL), and cyclohexane (7.5 mL) were first mixed together. Next, the mixture was continuously stirred for 10 min after 1.2 mL of H_2O were added. Then 80 μL of 0.1 M $Ru(bpy)_3^{2+}$ solution was introduced, followed by the addition of TEOS (200 μL) and NH_4OH (100 μL) to $Ru(bpy)_3^{2+}$-doped silica nanoparticles (Ru SNPs). After 18 h, Ru SNPs were amine-modified by adding 10 μL of APTES and then stirred for 20 h. After the modification, Ru SNPs were centrifuged, sonicated, and washed with 95% ethanol four times and finally dispersed in PBS solution (pH = 7.4, 0.1 M) for further use. To obtain Ru SNP-DNA probe, the following steps were performed.[40] One mg DSG was added into 100 μL of 1 mg/mL amine-modified Ru SNPs (PBS: pH = 7.4). After 2 h of stirring at 37 °C, the reaction mixture was centrifuged and vortexed four times with PBS. The resulting Ru SNPs-DSG were sonicated violently and then incubated with 2.9×10^{-7} M DNA probe in PBS solution (pH = 7.4, 0.1 M) for 3 h at 37 °C under the vortex condition, and washed three times with PBS. An Ru SNP had ~290 DNA strands, and the measurement method[41,42] is shown in the SI.

Preparation of ECL Immunosensor. In this work, the construction process of the PEDV antibody immunosensor was exhibited in Scheme 1. For the pretreatment of the glassy carbon electrode (GCE) of 3 mm diameter, they were first polished using 1.0 μm, 0.3 μm, and 0.05 μm alumina slurry (Beuhler) successively, and then washed thoroughly with deionized water. The polished GCE was sonicated in nitric acid solution (v_{HNO3}/v_{H2O} = 1:1) and deionized water and then dried with nitrogen air. For the construction process, first the GCE was dried in air for about 4 h after Au-GN hybrids (6 μL) were dropped on their surface. To remove the unabsorbed materials, the Au-GN/GCE was rinsed three times with PBST (0.02% Tween 20 in PBS, pH7.4). Then, the Au-GN/GCE was immersed in 60 μL of 50-fold diluted PEDV (Ag) suspension (0.01 M PBS, pH 7.4) and stored at 4 °C for 12 h. Next, the Ag/Au-GN/GCE was washed with PBST and incubated in 60 μL 0.5 wt % BSA solution at 37 °C for 1 h to block the nonspecific binding sites. After rinsing with PBST, the BSA/Ag/Au-GN/GCE was immersed in 60 μL PEDV antibody (Ab_1) solution. After 50 min of reaction at 37 °C, the Ab_1 was expected to be covalently bonded with PEDV. Finally, the Ab_1/BSA/PEDV/Au-GN/GCE was incubated in biotin-goat anti mouse IgG (B-Ab_2, 60 μL) for 60 min at 37 °C (here PEDV antibody is from mouse serum). The resulting electrodes (B-Ab_2/Ab_1/BSA/PEDV/Au-GN/GCE) were rinsed 3 times with PBST to remove the unbounded conjugates. After the reaction, the modified GCE were incubated in 60 μL streptavidin solution (10 nM) containing salmon sperm DNA (100 μg mL^{-1}) and 0.2% BSA for 30 min at 37 °C. After gently rinsing with PBST, the SA/B-Ab_2/Ab_1/BSA/PEDV/Au-GN/GCE were incubated in circularization mixture (60 μL) containing 40 nM biotinylated primer DNA and 40 nM circular template DNA and incubated at 37 °C for 30 min.

Rolling Circle Amplification and Ru-DNA Tagging. All types of DNAs were shown in Table S1. RCA reaction was started by incubating in reaction buffer (pH 7.5, 60 μL, 50 mM Tris-HCl buffer, containing 10 mM dNTP, 0.1% Tween 20, 33 mM potassium acetate, 10 mM magnesium acetate, and 1 mM dithiothreitol) with phi29 DNA polymerase (0.2 units) and then continued for 1 h at 37 °C after the modified GCE was rinsed gently with washing buffer. After RCA reaction was finished, the modified GCE was carefully washed with PBST. Next, 10 μL of 0.48 μM Ru-DNA probe was hybridized for 30 min at 37 °C after being dropped on the electrode. Finally, the modified GCE were rinsed with PBST to separate the nontagged Ru-DNA probe for the succeeding ECL characterization assays.

ECL Detection of the Constructed Immunosensor. When the modification procedures of PEDV antibody sensors were completed, the obtained immunosensors were investigated in a 5 mL homemade quartz cell, where modified GCE

DOI: 10.1021/acs.analchem.8b00853
Anal. Chem. XXXX, XXX, XXX−XXX

acted as a working electrode and performed in 0.1 M PBS (pH 7.4) containing 10 mM TPA at room temperature. The photomultiplier tube (PMT) voltage was proposed at 900 V, and the range of continuous potential was from 0 to 1.3 V at a scanning rate of 100 mV·s^{-1}.

RESULTS AND DISCUSSION

Characterization of Au-GN Hybrids and Ru SNP-DNA Probe. Graphene nanosheets (GN) have been widely used to fabricate the ECL platform due to their unique electron structure and chemical properties.[43,44] Due to their good electrocatalytic activity, excellent biocompatibility, and large surface area, gold nanoparticles (Au NPs) have also been widely used in the assembly of ECL biosensors.[45] In this work, Au-GN hybrids were used as the substrate to fabricate the biosensor for PEDV antibody detection. The morphologies of Au NPs and the Au-GN hybrids were characterized by TEM images (Figure 1A, B). In Figure 1A, Au NPs showed an average diameter of about 20 nm. There were large amounts of Au NPs loaded on the surface of the thin flake-like GN-PDDA as presented in Figure 1B, which revealed that Au NPs were well-dispersed on the surface of GN.

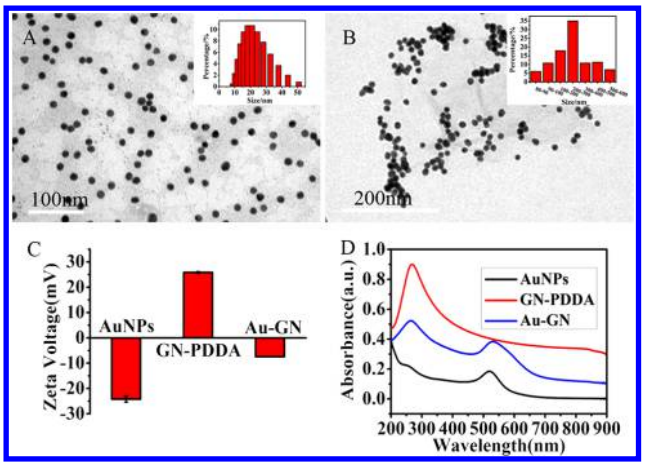

Figure 1. TEM image of (A) Au NPs (inset: size distribution of Au NPs), and (B) Au-GN hybrids (inset: size distribution of Au-GN). (C) Evolution of zeta potential of the Au-GN hybrids coupling process. (D) UV- vis absorption spectra of Au NPs, GN- PDDA, and Au-GN hybrids.

To further demonstrate this process, zeta potentials of the nanocomposites were recorded in Figure 1C. The mean zeta potential of GN-PDDA and Au NPs were +25.7 mV and −24.2 mV, respectively. After the GN-PDDA were mixed with Au NPs, the zeta potential changed to −7.39 mV. From the UV−vis absorption spectra (Figure 1D), it can be seen that the GN and Au NPs behaved characteristic peaks at 270 and 530 nm, respectively. After the formation of Au-GN hybrids, Au NPs showed a red shift at 530 nm and the characteristic peak of GN also appeared at 270 nm, which revealed the successful preparation of Au-GN composites.

In this work, the Ru SNPs were synthesized using a reverse microemulsion method according to previous literature.[39] As shown in Figure 2A, the obtained Ru SNPs were spherical and uniform with a diameter of ~24 nm. The preparation process of the Ru SNPs-DNA probe was depicted in Scheme 1A. The preparation result of Ru SNPs-NH_2 was shown in Figure 2B. FT-IR spectroscopy showed strong peaks at 790 cm^{-1}, 1084 cm^{-1} (Si−O−Si: ν_s and ν_{as}), 950 cm^{-1} (ν_{Si-OH}), and 460 cm^{-1} (δ_{O-Si-O}). After Ru SNPs were amino-functionalized, obvious changes can be seen for amino groups at 1640 cm^{-1} (δ_{NH}) and a stronger vibration peak at 3400 cm^{-1} (ν_{NH}). The results indicated that amino group were successfully modified on Ru SNPs. Moreover, the zeta potentials of Ru SNPs, Ru SNPs-NH_2, Ru SNPs-DSG, and Ru SNPs-DSG-DNA are described in Figure 2C. After the functionalization of the aminon group, the negatively charged (−12.5 mV) Ru SNPs came to bear positive charge (+8.97 mV). It could demonstrate that the amino-groups were successfully modified on Ru SNPs. Furthermore, when Ru SNPs-NH_2 were further modified with DSG, more aminon groups were attached, thus the value of the surface potential was obviously increased from +8.97 to +15.5 mV. However, when Ru SNPs-DSG were coupled with DNA, the surface potential significantly dropped to −14.3 mV, which demonstrated that the coupling process was successful. Furthermore, the absorption spectrum and the obvious emission peak of $Ru(bpy)_3^{2+}$ and Ru SNPs were around 455 nm and at 590 nm (Figures 1S and 2S). UV−vis absorption spectrum and photoluminescence (PL) spectra showed the similar characteristic peak about the Ru SNPs before and after the modification.

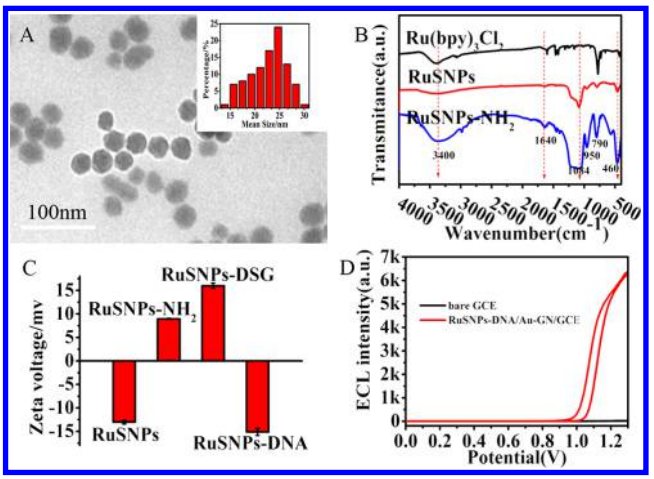

Figure 2. (A) TEM image of Ru SNPs (Inset: Size distribution of Ru SNPs). (B) FT-IR spectra of $Ru(bpy)_3Cl_2$ (black), Ru SNPs (red), and Ru SNPs-NH_2 (blue). (C) Evolution of zeta potential of the Ru SNPs-DNA coupling process. (D) ECL curves of Ru SNPs-DNA/Au-GN/GCE modified electrode.

Also, the ECL behavior of Ru SNPs-DNA was investigated in the presence of 10 mM TPA. The result was displayed in Figure 2D. It can be seen that no ECL peak appears on the bare GCE, however, one strong anodic ECL signal could be obtained when the electrode was modified with Ru SNPs-DNA. Therefore, Ru SNPs-DNA can be used as a nanoprobe for the ECL bioassay.

Characterization of the ECL-Sensing Platform. Cyclic voltammetry (CV) can provide electrochemical characteristics of modified electrodes. CVs could characterize the fabrication process of the ECL platform in electrolyte solution containing 0.1 M KCl and 5 mM $K_3Fe(CN)_6$. As shown in Figure 3A, compared with the bare electrode (curve a), the Au-GN modified electrode showed an obvious increament in CV current (curve b) due to the effective surface area and the excellent electron transfer acceleration capacity of Au-GN. When PEDV, BSA, Ab_1, bio-Ab_2, bio-DNA, and RCA products were successively immobilized onto the Au-GN/GCE, the redox peak current was declined in succession (curve c, d, e,

DOI: 10.1021/acs.analchem.8b00853
Anal. Chem. XXXX, XXX, XXX−XXX

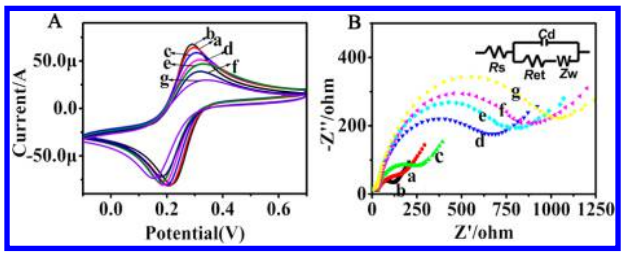

Figure 3. (A) Cyclic voltammograms and (B) the corresponding impedance curves for different fabricated steps: (a) GCE, (b) Au-GN/GCE, (c) Ag/Au-GN/GCE, (d) bio-Ab_2/Ab_1/BSA/Ag/Au-GN/GCE, (e) cDNA/SA/bio-Ab_2/Ab_1/BSA/Ag/Au-GN/GCE, (f) RCA/cDNA/SA/bio-Ab_2/Ab_1/BSA/Ag/Au-GN/GCE, and (g) Ru-DNA/RCA/cDNA/SA/bio-Ab_2/Ab_1/BSA/Ag/Au-GN/GCE in electrolyte solution containing 0.1 M KCl and 5 mM $K_3Fe(CN)_6$. Scan rate: 100 mV/s.

and f), which may be ascribed to the fact that protein and DNA are nonelectroactive materials and could severely hinder the diffusion of $[Fe(CN)_6]^{3-/4-}$. After incubation with the Ru-DNA-probe, the peak current still decreased (curve g) because the assembled Ru-DNA further impeded the electron transfer. The above results indicated the successful construction of the ECL sensing platform for PEDV antibody.

Moreover, EIS was also an excellent method to testify to the changes of the electrode surface. Normally, there is a linear portion and a semicircle portion in the Nyquist EIS spectrum. The diffusion limited process can be revealed by the linear portion at lower frequencies, and the electron transfer restricted process (Ret) can be reflected by the semicircle portion at higher frequency permeability.[46,47] As displayed in the Figure 3B, the different stages were presented with the Nyquist plots of the impedance spectrum, and the applied equivalent circuit was displayed in the inset. The Ret decreased from 87 Ω to 76 Ω when the Au-GN was modified on the electrode (curve b) because of the good conductivity of Au NPs and GN. Followed by the successive immobilization of PEDV, BSA, Ab_1, bion-Ab_2, SA, bio-DNA, RCA products, and Ru-DNA-probe, the resistance value continuously increased (curve c, Ret = 172 Ω; curve d, Ret = 492 Ω; curve e, Ret = 601 Ω; curve f, Ret = 668 Ω; curve d, Ret = 781 Ω) due to the poor conductivity of bioprotein molecules. All of the above-facts were in accordance with Figure 3A, indicating the successful fabrication of the PEDV antibody immunosensor.

The fluorescence microscopy images were also applied to verify the sandwiched immunoassay (SI Figure S3). ECL sensor was assembled on the electrode according to Scheme 1. As shown in Figure S3A, no fluorescence signal can be recognized on the electrode because there is no rolling circle amplification when the sensor was constructed. After rolling circle amplification, RuSNPs DNA probe could be easily attached on the linearly concatenated RCA products. Thus, obvious fluorescence signals can be observed on the assembled electrode. Therefore, it further revealed that the Ab_1 could specifically combine with PEDV.

In the assay, the RCA process had a great influence on the performance of the biosensor. Hence, agarose gel electrophoresis was performed to demonstrate the RCA reaction. As shown in Figure S4, the RCA products were observed in lane 2, and it showed an extremely low mobility, which was consistent with the fact that RCA products have the high molecular weight. However, the high molecular products did not appear in lane 1 in the negative control experiment. To further confirm the specific binding of long single strand DNA with Ru-DNA probes, RCA products combined with Ru SNPs-DNA were characterized by TEM (Figure S5). As shown in Figure S5A, the DNA probe modified Ru SNPs were well dispersed. After Ru-DNA probes bound specifically to the long strand linear DNA, they appeared as linear and branched structures (Figure S5B). The cause of the branched structures was due to the flexibility of single stranded DNA.[48] Ru-DNA probes could be bound specifically to the long strand linear DNA through the flexible DNA enveloping on the surface of the Ru-SNPs. The length of products could reach a few micrometers. Furthermore, to verify that the stereospecific blockade of Ru SNPs should have little effect on the combined efficiency of DNA probe with RCA products, the ECL response of the designed biosensor using the Ru SNPs-DNA nanotags was compared with using the Ru SNPs- mismatch-DNA. As shown in Figure S6, the ECL intensity using the Ru SNPs-DNA (curve b) as nanotags was much larger than that using the Ru SNPs-mismatch-DNA (curve a) as signal label. All the results indicated that the RCA reaction could be used to amplify the signal in immunoassay.

Optimization of the Detection Conditions. To acquire optimal ECL test conditions, the main conditions including the concentration of the Ru-DNA-probe (Figure 4A), the pH of

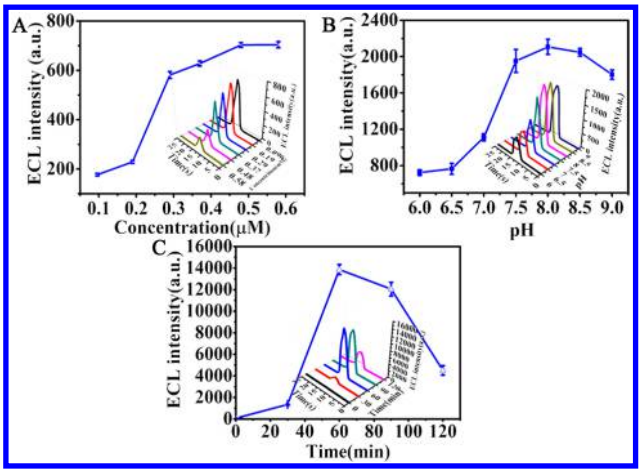

Figure 4. Effects of (A) concentrition of Ru SNPs-DNA-probe (0.096, 0.19, 0.29, 0.37, 0.48, and 0.58 μM). (RCA reaction time: 30 min; 10 pg mL^{-1} PEDV antibody solution). The ECL intensity was detected in PBS solution (0.1 M, 4 mL, pH 7.4, 10 mM TPA). (B) The value of pH (pH 6.0, 6.5, 7.0, 7.5, 8.0, 8.5, and 9.0) on ECL response of immunosensor. Working buffer was PBS solution (RCA reaction time: 60 min, 10 pg mL^{-1} PEDV Ab_1, 10 mM TPA). (C) RCA reaction time (0, 30, 60, 90, and 120 min) on ECL response of immunosensor (10 ng mL^{-1} PEDV Ab_1). Working buffer was PBS solution (4 mL, 0.1 M, pH 8.0, 10 mM TPA).

electrolyte solution (Figure 4B), and RCA time (Figure 4C) were optimized. Figure 4A exhibited the ECL behavior of the platform in known concentrations of Ru-DNA. As expected, the ECL response was increased promptly with the amplification of Ru-DNA. However, the ECL response tended to a constant value when the Ru-DNA concentration was 0.48 μM. As a result, the most suitable Ru-DNA concentration of 0.48 μM was adopted in the following experiments.

The pH of the electrolyte solution was researched to discuss its influence on the coreactant. TPrA on the electrode is oxidized into $TPrA^{+}$ and $TPrA^{\cdot}$. The reaction of $Ru(bpy)_3^{2+}$

DOI: 10.1021/acs.analchem.8b00853
Anal. Chem. XXXX, XXX, XXX−XXX

and $TPrA^{\cdot}$ produces $Ru(bpy)_3^{3+}$, which reacts with $TPrA^{\cdot+}$ to generates $Ru(bpy)_3^{2+*}$. The deprotonations of $TPAH^+$ and $TPrA^{\cdot+}$ governed by the pH of the electrolyte solution. So as depicted in Figure 4B, the ECL intensity increased with the increasing of the pH value of detection solution, and it tended to be a maximum value when the pH value was 8.0. The ECL intensity with a pH of greater than 8 tended to decline, which was probably ascribed to the instability of $Ru(bpy)_3^{3+}$ and the quenching effect of oxygen produced by water in high pH solution when the potential is above 1.0 V.[49]

Finally, the effect of RCA reaction time on the ECL signal was also discussed to produce more complementary sequences of the circular template for generating enhanced signal amplification. Within the initial 30 min, the response of ECL was very weak, indicating that the rate of RCA reaction was relatively slow (Figure 4C). The quantities of RCA products increased with the increasing of amplification time, thus leading to the increment of the ECL intensity. The intensity increased rapidly after 30 min and reached the highest point at 60 min with the increasing RCA reaction time. But after 60 min, the intensity dropped down dramatically, which may be caused by inactivation of the phi 29 DNA polymerase or the saturation of the RCA product, or the excessively long DNA strand producing a large space resistance. Thus, the optimum time for the RCA reaction was chosen as 60 min in the following experiments.

ECL Analysis of the PEDV Antibody. Under the optimal conditions, the quantitative analysis of PEDV antibody was achieved by the proposed ECL biosensor based on Ru-DNA nanotags. As displayed in Figure 5A, the ECL intensity

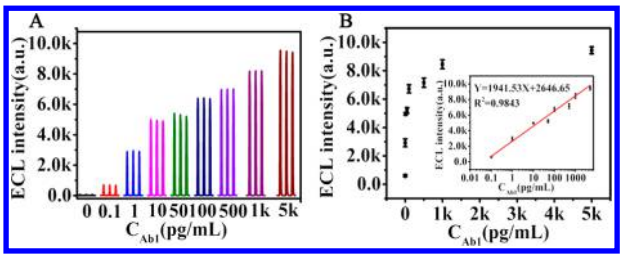

Figure 5. (A) The response of ECL intensity of RCA with different concentrations of PEDV antibody. (B) Calibration plot of the ECL intensity and the logarithm of the PEDV antibody concentrations.

increased with the increasing of PEDV antibody concentration. From Figure 5B, the calibration plot displayed a good linear relationship between the logarithm of the PEDV antibody concentrations from 0.1 pg mL^{-1} to 5000 pg mL^{-1} and ECL intensity. The linear regression equation was put as I_{ECL} = 1941.53 log C_{Ab1} + 2646.65 with the correlation coefficient of R = 0.9843, where I_{ECL} represented the ECL response and C_{Ab1} represented the concentration of the PEDV antibody. In addition, the detection limit of the PEDV antibody was 0.05 pg mL^{-1} (S/N = 3). In this regard, the proposed ECL biosensor showed high sensitivity, low detection limit, and wide linear range, suggesting it was an effective tool for the sensitive detection of the PEDV antibody.

Analysis of PEDV Antibody in Swine Serum. To discuss the feasibility of the ECL-sensing platform in clinical applications, PEDV antibody in swine serum was adopted as real samples in the detection. The diluted negative serum samples and the diluted positive serum (from a piglet infected with PEDV) were analyzed by the proposed method (Table S2). In addition, the experimental results were verified by the standard addition method. The RSD and recovery of the ECL immunoassay at different diluted concentrations of the PEDV antibody are listed in Table 1. It shows that the detection results of the PEDV antibody were in good agreement with those from the commercial ELISA test. The recoveries of the samples were from 106.2% to 107.2%, and the RSD was 1.9–6.3% for the PEDV antibody (n = 3), which demonstrated that the developed ECL platform could be used in the quantitative analysis of actual biological samples.

Specificity, Repeatability, and Stability of the ECL Platform. To investigate the selectivity and specificity of the ECL platform, several other proteins, including bovine serum albumin (BSA), immunoglobulin G (IgG), porcine circovirus (PCV), porcine reproductive and respiratory syndrome viruse (PRRSV), and Enterovirus-71 (EV-71) were tested as interference factors to make a distinction between PEDV and other proteins. As shown in Figure 6A, BSA (1%), IgG (10 pg/

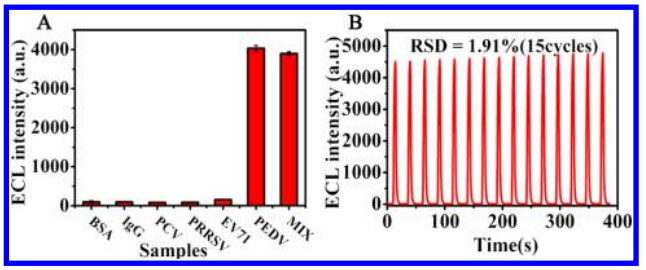

Figure 6. (A) Histogram for the specificity of this method for PEDV antibody detection: BSA (1%), IgG (10 pg/mL), PCV (10 pg/mL), PRRSV (10 pg/mL), EV71 (10 pg/mL), PEDV (10 pg/mL), and a mixture containing 10 pg/mL BSA, 10 pg/mL IgG, 10 pg/mL PCV, 10 pg/mL PRRSV, 10 pg/mL EV71, and 10 pg/mL PEDV. (B) Stability of the proposed method under consecutive 15 cyclic potential scans. The potential scanning was set from 0 to 1.3 V with a scan rate of 0.1 V/s.

mL), PCV (10 pg/mL), PRRSV (10 pg/mL), and EV71 (10 pg/mL) were used to perform the control experiments, respectively. No obvious ECL signal was observed when PEDV was replaced by BSA, IgG, PCV, PRRSV, and EV71. Moreover, the mixture of PEDV with BSA, IgG, PCV, PRRSV, and EV71 appeared with ECL intensity, approximating that of the standard PEDV sample. The above results revealed that BSA, IgG, PCV, PRRSV, and EV71 had negligible influence on

Table 1. Recoveries of PEDV Antibody from the Serum Detected by the Proposed Immunosensor (n = 3)

		found (pg/mL)			ELISA
sample no.	added (pg/mL)	($x \pm s$, n = 3)	R. SD (%)	recovery (%)	($x \pm s$, n = 3)
1	0	2.9 ± 0.1			3.2 ± 1.1
2	10	13.1 ± 0.1	1.9	107.2	14.2 ± 1.6
3	20	23.1 ± 1.2	6.3	106.2	24.3 ± 2.1

DOI: 10.1021/acs.analchem.8b00853
Anal. Chem. XXXX, XXX, XXX−XXX

the response to PEDV, which manifested good selectivity and specificity of the sensing platform.

Stability of the ECL-sensing platform is an important factor in practical applications. The continuous ECL scans of 15 cycles were monitored to study the stability of the sensing platform (with 10 pg/mL PEDV) in 0.1 M PBS (pH = 8) under the optimum conditions. As displayed in Figure 6B, the proposed ECL biosensor presented favorable stability with the relative standard deviation (RSD) of 1.91%, revealing that the ECL signal was relatively constant. The reproducibility of the biosensor was another important feature for the PEDV antibody detection. Therefore, the reproducibility of the experimental method was studied by comparing the ECL intensity of three different electrodes, and the obtained RSD was 3.9%. Furthermore, the ECL signal intensity of the same biosensor was 91.9% of the original value after stored at 4 °C for 1 week, which indicated that the sensor had a good reproducibility.

CONCLUSIONS

Using the antibody−antigen reaction as the recognition unit, rolling circle amplification (RCA) for signal enhancement, assembled cascade Ru-DNA nanotags as signal label, and Au NP modified graphene nanosheet (Au-GN) as substrate, a versatile cascade ECL signal amplification sensing platform was developed to monitor the PEDV antibody. The streptavidin-modified assembler cascade DNA probe and $Ru(bpy)_3^{2+}$-doped silica nanoparticles were applied in the field of ECL sensing for PEDV antibody for the first time, which obtained high stability and high sensitivity. Moreover, the proposed ECL biosensor presented satisfied applicability for PEDV antibody detection, which indicated that the proposed ECL biosensor might be a powerful research tool in analytical chemistry, virus research, and other related fields.

ASSOCIATED CONTENT

Supporting Information

The Supporting Information is available free of charge on the ACS Publications website at DOI: 10.1021/acs.analchem.8b00853.

Experimental details; oligonucleotide sequences used in this work; UV−vis absorption spectra and PL spectra of ruthenium nanocomposites; fluorescence microscope images; agarose gel electrophoresis experiments; TEM images of Ru SNPs-DNA and Ru SNPs tagged RCA products; the ECL response using the Ru SNPs-mismatch-DNA and the Ru SNPs-DNA as signal label; and comparative data of the ECL assay and indirect ELISA assay of serum samples (at a dilution ratio of 1:200) (PDF)

AUTHOR INFORMATION

Corresponding Author

*Fax: (+86)-027-8728 8505. E-mail: hyhan@mail.hzau.edu.cn (H.H.).

ORCID

Heyou Han: 0000-0001-9406-0722

Notes

The authors declare no competing financial interest.

ACKNOWLEDGMENTS

This research was financially supported by National Key R&D Program (2016YFD0500706) and National Natural Science Foundation of China (21778020), Sci-tech Innovation Foundation of Huazhong Agriculture University (2662017PY042, 2662018PY024).

REFERENCES

(1) Chen, Q.; Li, G. W.; Stasko, J.; Thomas, J. T.; Stensland, W. R.; Pillatzki, A. E.; Gauger, P. C.; Schwartz, K. J.; Madson, D.; Yoon, K. J. *J. Clin. Microbiol.* **2014**, *52*, 234−243.
(2) Gao, Y.; Kou, Q.; Ge, X.; Zhou, L.; Guo, X.; Yang, H. *Arch. Virol.* **2013**, *158*, 711−715.
(3) Hou, Y.; Lin, C. M.; Yokoyama, M.; Yount, B. L.; Marthaler, D.; Douglas, A. L.; Ghimire, S.; Qin, Y.; Baric, R. S.; Saif, L. J.; Wang, Q. *J. Virol.* **2017**, *91*, e00227-17.
(4) Huang, Y. W.; Dickerman, A. W.; Pineyro, P.; Li, L.; Fang, L.; Kiehne, R.; Opriessnig, T.; Meng, X. J. *mBio* **2013**, *4*, e00737-13.
(5) Ren, X.; Suo, S.; Jang, Y. S. *Biotechnol. Lett.* **2011**, *33*, 215−220.
(6) Zeng, S. L.; Zhang, H.; Ding, Z.; Luo, R.; An, K.; Liu, L. Z.; Bi, J.; Chen, H. C.; Xiao, S. B.; Fang, L. R. *Proteomics* **2015**, *15*, 1819−1828.
(7) Richter, M. *Chem. Rev.* **2004**, *104*, 3003−3036.
(8) Miao, W. J. *Chem. Rev.* **2008**, *108*, 2506−2553.
(9) Wu, Z.; Hu, J.; Zeng, T.; Zhang, Z. L.; Chen, J. J.; Wong, G.; Qiu, X. G.; Liu, W. J.; Gao, G. F.; Bi, Y. H.; Pang, D. W. *Anal. Chem.* **2017**, *89*, 2039−2048.
(10) Zhou, Y.; Yan, D.; Wei, M. *J. Mater. Chem. C* **2015**, *3*, 10099−10106.
(11) Babamiri, B.; Hallaj, R.; Salimi, A. *Biosens. Bioelectron.* **2018**, *99*, 353−360.
(12) Shao, K.; Wang, J.; Jiang, X. C.; Shao, F.; Li, T. T.; Ye, S. Y.; Chen, L.; Han, H. Y. *Anal. Chem.* **2014**, *86*, 5749−5757.
(13) Cui, C.; Chen, Y.; Jiang, D. C.; Zhu, J. J.; Chen, H. Y. *Anal. Chem.* **2017**, *89*, 2418−2423.
(14) Wu, L.; Ding, F.; Yin, W. M.; Ma, J.; Wang, B. R.; Nie, A. X.; Han, H. Y. *Anal. Chem.* **2017**, *89*, 7578−7585.
(15) Xu, Z. Q.; Liao, L. L.; Chai, Y. Q.; Wang, H. J.; Yuan, R. *Anal. Chem.* **2017**, *89*, 8282−8287.
(16) Zhang, H. R.; Li, B. X.; Sun, Z. M.; Zhou, H.; Zhang, S. S. *Chem. Sci.* **2017**, *8*, 8025−8029.
(17) Zhang, X.; Zhang, B.; Miao, W. J.; Zou, G. Z. *Anal. Chem.* **2016**, *88*, 5482−5488.
(18) Jiang, X. Y.; Wang, H. J.; Wang, H. J.; Yuan, R.; Chai, Y. Q. *Anal. Chem.* **2016**, *88*, 9243−9250.
(19) Wen, W.; Yan, X.; Zhu, C. Z.; Du, D.; Lin, Y. H. *Anal. Chem.* **2017**, *89*, 138−156.
(20) Sardesai, N. P.; Barron, J. C.; Rusling, J. F. *Anal. Chem.* **2011**, *83*, 6698−6703.
(21) Feng, Y. Q.; Sun, F.; Wang, N. N.; Lei, J. P.; Ju, H. X. *Anal. Chem.* **2017**, *89*, 7659−7666.
(22) Wang, Y. G.; Zhao, G. H.; Li, X. J.; Liu, L.; Cao, W.; Wei, Q. *Biosens. Bioelectron.* **2018**, *101*, 290−296.
(23) Afsharan, H.; Navaeipour, F.; Khalilzadeh, B.; Tajalli, H.; Mollabashi, M.; Ahar, M. J.; Rashidi, M. R. *Biosens. Bioelectron.* **2016**, *80*, 146−153.
(24) Chen, Z. H.; Liu, Y.; Wang, Y. Z.; Zhao, X.; Li, J. H. *Anal. Chem.* **2013**, *85*, 4431−4438.
(25) Wang, X. Y.; Zhou, J. M.; Yun, W.; Xiao, S. S.; Chang, Z.; He, P. G.; Fang, Y. Z. *Anal. Chim. Acta* **2007**, *598*, 242−248.
(26) Qian, J.; Zhou, Z. X.; Cao, X. D.; Liu, S. Q. *Anal. Chim. Acta* **2010**, *665*, 32−38.
(27) Zhang, W.; Xiong, H. W.; Chen, M. M.; Zhang, X. H.; Wang, S. F. *Biosens. Bioelectron.* **2017**, *96*, 55−61.
(28) Joffroy, B.; Uca, Y. O.; Prešern, D. N.; Doye, J. P. K.; Schmidt, T. L. *Nucleic Acids Res.* **2018**, *46*, 538−545.
(29) Li, F.; Zhang, H.; Wang, Z.; Newbigging, A. M.; Reid, M. S.; Li, X. F.; Le, X. C. *Anal. Chem.* **2015**, *87*, 274−292.

DOI: 10.1021/acs.analchem.8b00853
Anal. Chem. XXXX, XXX, XXX−XXX

(30) Wang, Q.; Gan, X.; Zang, R.; Chai, Y.; Yuan, Y.; Yuan, R. *Biosens. Bioelectron.* **2016**, *81*, 382−387.
(31) Li, S. K.; Chen, A. Y.; Niu, X. X.; Liu, Z. T.; Du, M.; Chai, Y. Q.; Yuan, R.; Zhuo, Y. *Chem. Commun.* **2017**, *53*, 9624−9627.
(32) Ke, R.; Nong, R. Y.; Fredriksson, S.; Landegren, U.; Nilsson, M. *PLoS One* **2013**, *8*, e69813.
(33) Chen, K.; Wu, L.; Jiang, X.; Lu, Z.; Han, H. *Biosens. Bioelectron.* **2014**, *62*, 196−200.
(34) Osterberg, F. W.; Rizzi, G.; Donolato, M.; Bejhed, R. S.; Mezger, A.; Stromberg, M.; Nilsson, M.; Stromme, M.; Svedlindh, P.; Hansen, M. F. *Small* **2014**, *10*, 2877−2882.
(35) Liu, X.; Song, M.; Hou, T.; Li, F. *ACS Sensors* **2017**, *2*, 562−568.
(36) Frens, G. *Nature, Phys. Sci.* **1973**, *241*, 20−22.
(37) Kovtyukhova, N. I.; Ollivier, P. J.; Martin, B. R.; Mallouk, T. E.; Chizhik, S. A.; Buzaneva, E. V.; Gorchinskiy, A. D. *Chem. Mater.* **1999**, *11*, 771−778.
(38) Liu, K.; Zhang, J.; Yang, G.; Wang, C.; Zhu, J. J. *Electrochem. Commun.* **2010**, *12*, 402−405.
(39) Song, Y.; Du, D.; Li, L.; Xu, J.; Dutta, P.; Lin, Y. H. *ACS Appl. Mater. Interfaces* **2017**, *9*, 20410−20416.
(40) Bae, S. W.; Cho, M. S.; Hur, S. S.; Chae, C. B.; Chung, D. S.; Yeo, W. S.; Hong, J. I. *Chem. - Eur. J.* **2010**, *16*, 11572−11575.
(41) Liu, B. W.; Wu, P.; Huang, Z. C.; Ma, L. Z.; Liu, J. W. *J. Am. Chem. Soc.* **2018**, *140*, 4499−4502.
(42) Demers, L. M.; Mirkin, C. A.; Mucic, R. C.; Reynolds, R. A.; Letsinger, R. L.; Elghanian, R.; Viswanadham, G. *Anal. Chem.* **2000**, *72*, 5535−5541.
(43) Dong, Y. P.; Zhou, Y.; Wang, J.; Zhu, J. J. *Anal. Chem.* **2016**, *88*, 5469−5475.
(44) Pumera, M. *Chem. Soc. Rev.* **2010**, *39*, 4146−4157.
(45) Guo, S. J.; Wang, E. K. *Anal. Chim. Acta* **2007**, *598*, 181−192.
(46) Lu, H. Y.; Hu, N. F. *Electroanalysis* **2006**, *18*, 1511−1522.
(47) Fan, G. C.; Han, L.; Zhang, J. R.; Zhu, J. J. *Anal. Chem.* **2014**, *86*, 10877−10884.
(48) Gu, Y.; Zhang, T. T.; Huang, Z. F.; Hu, S. W.; Zhao, W.; Xu, J. J.; Chen, H. Y. *Chem. Sci.* **2018**, *9*, 3517−3522.
(49) Gao, W.; Xia, X. H.; Xu, J. J.; Chen, H. Y. *J. Phys. Chem. C* **2007**, *111*, 12213−12219.

DOI: 10.1021/acs.analchem.8b00853
Anal. Chem. XXXX, XXX, XXX−XXX